

NEW GLOBAL MARS CONTROL POINT NETWORK *

Timm Ohlhof
System Development, Reconnaissance and Remote Sensing Systems
ESG Elektroniksystem- und Logistik-GmbH
P.O.B. 80 05 69, D-81605 Munich, Germany
Phone: +49-89-9216 2285, Fax: +49-89-9216 2732, e-mail: tohlhof@esg-gmbh.de

Wolfgang Zeitler
Institute of Planetary Exploration
German Aerospace Center e.V. (DLR)
Rudower Chaussee 5, D-12489 Berlin, Germany
Phone: +49-30-67055 398, Fax: +49-30-67055 303, e-mail: Wolfgang.Zeitler@dlr.de

Heinrich Ebner
Chair for Photogrammetry and Remote Sensing, Technische Universität München
D-80290 Munich, Germany
Phone: +49-89-2892 2671, Fax: +49-89-280 95 73, e-mail: ebn@photo.verm.tu-muenchen.de

Commission IV, Working Group IV/5

KEY WORDS: Mars, Viking, bundle block triangulation, control point network

ABSTRACT

This paper deals with the computation of a new global control point network of the planet Mars. The existing Mars control point net is based on Viking data and consists of a large number of ground points, which can be easily identified in the imagery and whose 3-dimensional object coordinates (e.g. latitude φ , longitude λ and height h w.r.t. a reference ellipsoid) are known. These coordinates were now determined again to eliminate several disadvantages of former computations and to include the currently best available input data like improved Viking trajectory information, the Viking occultation data, present rotational parameters and the Mars Pathfinder lander.

Within a simultaneous 3D bundle block triangulation, 7 interior orientation parameters, the position and attitude parameters of 1140 images and the ground coordinates of 3739 tie points and 1 control point were estimated. The rms values $\mu_{\hat{X}}$, $\mu_{\hat{Y}}$, $\mu_{\hat{Z}}$ of the theoretical standard deviations of the adjusted object coordinates amount to 750 m, 770 m and 710 m, which is a significant improvement compared with former results (1–5 km). The accuracy of the ground point coordinates is close to the theoretical accuracy limit of 520 m in X , Y and Z , where error-free orientation parameters are assumed.

This new set of orientation parameters and ground points may now be used for local, regional and global DTM generation, the determination of reference bodies, mapping purposes as well as for current (Mars Global Surveyor 1996) and future (e.g. Mars Surveyor 1998 and 2001, Mars Express 2003) missions to Mars.

1 INTRODUCTION

A very important part of the description of a planet is its exact shape and size. Shape and size are usually derived from a ground point network, which contains a large number of globally distributed points on the planetary surface. The coordinates of these ground points are in general determined by photogrammetric methods. The ground point net characterizes the local, regional and global shape of the planet and serves as a basis for the computation of reference bodies such as spheres, 2-axial and 3-axial ellipsoids, or spherical harmonic functions.

Since all ground points are determined simultaneously in a common body-fixed object coordinate system together with the orientation parameters of the included images, they provide necessary control information for topographic mapping. Geocoded image maps can be compiled using the ground control point coordinates and the position and attitude parameters of the images. Additionally, local networks based on high resolution images can be tied to the global frame, when selected points from the global net are used as control points. Of course, all digital terrain models are based on the ground control net computation, since the required orientation parameters are taken from the block triangulation.

After a review of the existing control point networks on Mars the data sources for the new global Mars network are described. The

results of the block triangulation are presented and discussed in detail. Finally, a summary and an outlook are given.

2 EXISTING CONTROL POINT NETWORKS ON MARS

For building up a planetwide control point network on Mars, it is first necessary to define its body-fixed coordinate system. The small crater Airy-0 has been chosen to define the prime meridian of Mars. According to the direction of Mars' rotation, west longitude is used. The reference body for Mars is an ellipsoid of revolution (spheroid) with an equatorial radius of 3393.4 km and a polar radius of 3375.8 km (de Vaucouleurs et al., 1973).

The first control point network on Mars was computed in the early 1970's by M. Davies from RAND Corp. based on Mariner 6 and 7 image data (Davies and Berg, 1971). In the following years, images from the missions Mariner 9 and Viking 1 and 2 were taken and the number of points has increased. Finally, 9585 control points were measured in 1054 Mariner 9 images and 1555 Viking Orbiter 1 and 2 images (Davies, 1993). Most of these points are centers of craters defined by their rims (Fig. 1).

The former block adjustments were performed on a regional level, where the planimetric coordinates φ and λ of each point as well as the 3 orientation angles of each image were estimated, whereas the height coordinates h of the points and the position parameters of the images were treated as constants. The accuracy of the φ

*submitted to *Photogrammetric Engineering and Remote Sensing*

and λ coordinates is about 1 km up to 30° from the equator and 3–6 km from 30° towards the poles. In addition, the two Viking landing sites were located via Doppler tracking with an accuracy of about 100 m (Michael Jr., 1979). One of them was identified in two high resolution (8 m/pixel) Viking Orbiter images and could be located with an accuracy of 50 m by correlating topographic features between Viking Orbiter and Lander 1 images (Morris and Jones, 1980). The high resolution Orbiter images were tied to the low resolution Orbiter images of the ground point net by a local network of about 30 common points.

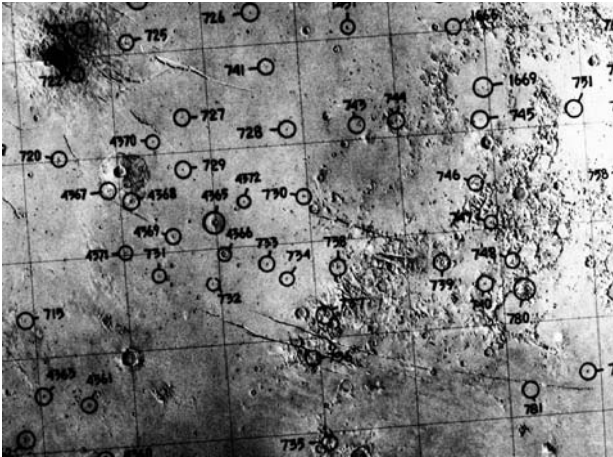


Figure 1: Ground control points on Mars (Davies et al., 1978)

The height datum of Mars is defined by the gravity field and the zero elevation as lying where the mean atmospheric pressure is equal to the triple point of water (6.1 mbar). For a systematic mapping of the Mars topography at 1:2 Mio. scale with 1 km contours, S. Wu from U.S. Geological Survey (USGS) compiled in the 1980's a separate 3D control point network with a total of 4502 points in 1157 Viking Orbiter 1 and 2 images (Wu and Doyle, 1990). This USGS net was based on Davies' planimetric net from 1978 (Davies et al., 1978), with elevations w.r.t. the Mars 6.1 mbar height datum. The adjustment of this second global network was performed in 5 separate block triangulations, and the single blocks were then connected to a global network. In this work occultation measurements from the Mariner 9 and Viking S-Band radio experiments and elevations derived from Earth-based radar profiles were incorporated as well. The accuracy of the object point coordinates is about 4 km in planimetry and 800 m in height.

These two existing ground point networks have in today's view several drawbacks. Both networks were computed based on the original Viking SEDR (Supplemental Experimenter Data Record) trajectory information for the image positions, but in the meantime it was found that this dataset contains large systematic errors in the order of 20 km, due to less precise planetary ephemeris and Mars gravity field coefficients (for more details see section 3.5). During the Viking orbit revision it became clear that the image time tags, i.e. the recording times of the Viking Orbiter images, are erroneous too, up to a few seconds. Note that a time error of 1 s causes an along-track position error of about 10 km depending on the velocity of the spacecraft. Furthermore, we found that the given interior orientation parameters (esp. the calibrated focal lengths c) of the 4 Viking Orbiter cameras are affected by systematic errors. Another error source are the image coordinates of the tie points, which were measured manually on analytical plotters. About 20% of the image points had to be removed in several pre-adjustments because of the large residuals of their image coordinates. All points which appear in 2 images only (2-ray points) were excluded too, due to their poor reliability.

The Mars Pathfinder mission has yielded much new information including the object coordinates of its landing site and improved Mars rotational parameters (MRP). Additionally, the Viking S-Band radio

occultation data were re-analysed by a research group at NASA's Goddard Space Flight Center (Smith and Zuber, 1996), and this improved dataset was included in the new adjustment. Finally, the USGS network was computed in separate block triangulations due to the lack of computer power. With the help of present day powerful workstations, however, the whole global block was adjusted in one single step within a reasonable time (ca. 5–10 h).

3 DATA SOURCES

3.1 Tie points

The existing USGS ground point network of Mars is based on images of the two Viking Orbiters (VO) 1 and 2 launched in 1975. After hundreds of orbits 97% of the surface of Mars were covered by more than 52,000 images. For the USGS network, 1157 low resolution images with a ground pixel size of 700–900 m were selected to provide sufficient overlap between adjacent images as well as a good global coverage. In these images many tie points were measured, mainly centers of craters. We selected 16,711 (88.1%) out of the original 18,976 image points after several pre-adjustments. Most points were rejected due to large residuals of the image coordinates, and all 2-ray points were removed too. All further computations were based on this consistent subset of USGS Viking image coordinates.

The most prominent points on Mars, Viking Lander 1 (VL1), Mars Pathfinder (MPF) and Airy-0, which can serve as control points, are not included within the USGS dataset. The landing of Mars Pathfinder in July 1997 provides us with a new ground control point (GCP). The 3D object coordinates of the landing site were derived by tracking methods, while the landing site itself could be identified in high-resolution Viking images (40 m ground pixel size) with a precision of about 1 pixel. Around all three points local networks were established. To this end, image coordinates of M. Davies (VL1 and Airy-0), T. Duxbury (MPF) and J. Oberst (MPF) were checked carefully and then combined with the USGS image coordinates by local networks of about 30 common tie points. Unfortunately, VL2 could not be identified in Viking images.

Moreover, we found out that the existing image coordinates of VL1 are erroneous because a wrong point on Mars was measured. For the correct point (= VL1) no image coordinates are available up to now. Therefore, VL1 was treated as an additional tie point.

As result, we have now a consistent and reliable set of image coordinates from 3739 tie points and 1 control point (Fig. 2), where VL1 and Airy-0 are tie points. This dataset consists of a total of 16,711 image points measured in 1138 VO 1 and 2 images and 2 Mariner 9 images due to Airy-0.

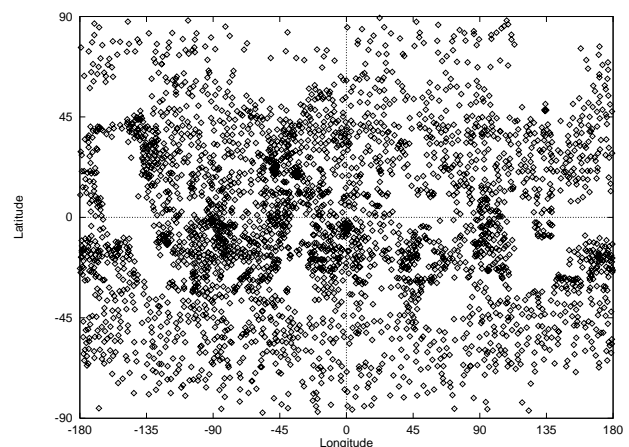


Figure 2: Distribution of 3739 tie points and 1 control point (MPF) of the new global Mars network

3.2 Control points

In the course of a combined non-photogrammetric adjustment using the original tracking data of both Viking Landers and the new Pathfinder data, inertial coordinates of all three landers were estimated very accurately with $\sigma = 30$ m (Folkner et al., 1997). The MPF coordinates were then transformed into body-fixed XYZ-coordinates and introduced into the bundle block adjustment.

The small crater Airy-0 (500 m diameter) defines the prime meridian ("Greenwich") on Mars, thus its Y -coordinate should be included with $\sigma = 0.0$ m in the bundle block adjustment. After the slight revision of the MRP by the Mars Pathfinder team the 0° meridian, however, does not cross the crater Airy-0. Therefore Airy-0 can't be used as a GCP any longer.

3.3 Radio occultation data

When a spacecraft is occulted by a planet, the radio signal is lost, and it appears again when it emerges from behind the planet. The knowledge of the ephemeris of Mars and Earth, the time and location of the loss of the signal give estimates of the radius r of the planet at the occultation point. Earlier studies (Smith and Zuber, 1996) re-analysed the Viking S-Band occultation data using the best current models for the planetary ephemeris and atmosphere. As result, 368 surface points were computed with their coordinates φ , λ and r . The standard deviations of the radii vary between 200 m and 1200 m, with an rms value of 500 m. In our study, 246 of these points were finally incorporated.

3.4 Earth-based radar data

From Earth-based radar observations the Mars radii can be derived along profiles near the equator ($\phi \pm 25^\circ$) with an accuracy of about 300 m. About 1000 radar points were used in the USGS network at that time. Since the 1980's, many additional Earth-based radar observations were made, but these information have been not included in any Mars network until now. In our block triangulation no radar data were used.

3.5 Orbit and attitude information

During the orbit revision effort, it became clear that many Viking time tags were erroneous for some unrecoverable reasons. Therefore efforts were made to reconstruct the times when the images were acquired as well as possible. In this study, we used the results of these efforts to compute the position and attitude parameters of the images.

Trajectory data of both VO spacecrafts were derived from the orbit revision project (Konopliv and Sjogren, 1995). The accuracy of the new orbit trajectories was increased from 2 km to a level of 500 m related to inertial space, due to the availability of the better Mars gravity field model Mars50c and a more precise model of the planetary ephemeris (DE234). All Viking S-Band tracking data were now processed simultaneously while the old SEDR data were collected and processed piecewise during the mission as the data were received.

A comparison between the old and new trajectories was performed by computing the VO spacecraft positions at the same image time tags using both orbit informations. The differences between the resulting positions amount to 20 km on average, which gives an indication of the systematic errors within the old SEDR data (Fig. 3 and 4). In this study, we used the new orbit data to compute the positions of the images.

The original Viking attitude data which comprise the three orientation angles for each image were introduced into the adjustment without any modifications. Due to their poor accuracy (0.25 gon), they are of limited use.

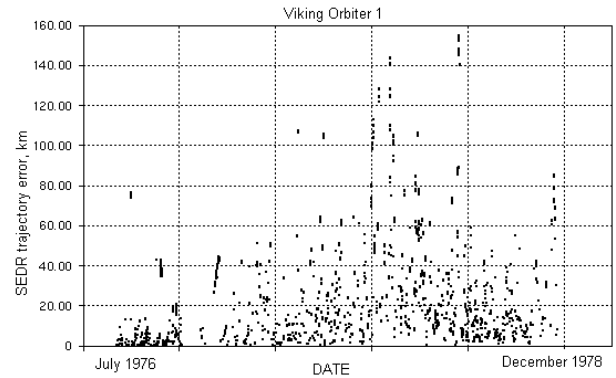


Figure 3: Differences between old and new Viking Orbiter 1 trajectories

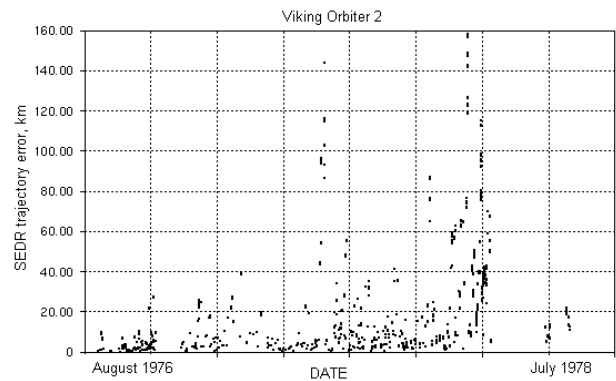


Figure 4: Differences between old and new Viking Orbiter 2 trajectories

3.6 Mars rotation parameters

As mentioned earlier, the rotational parameters of Mars were improved after the landing of Pathfinder. We used this information to convert the position and attitude parameters of the images, given in inertial space, into the Mars-fixed, non-inertial coordinate system XYZ . The following values were introduced (Folkner et al., 1997):

$$\alpha = \alpha_0 + \dot{\alpha}T = 317.9681431 - 0.10617 T \quad (1)$$

$$\delta = \delta_0 + \dot{\delta}T = 52.9886503 - 0.06094 T \quad (2)$$

$$W = W_0 + \dot{W}d = 176.901 + 350.891982268 d \quad (3)$$

with

- α : Right ascension of the Mars north pole
- α_0 : Right ascension of the Mars north pole at epoch J2000
- $\dot{\alpha}$: Right ascension rate
- δ : Declination of the Mars north pole
- δ_0 : Declination of the Mars north pole at epoch J2000
- $\dot{\delta}$: Declination rate
- W : Orientation of the Mars prime meridian
- W_0 : Orientation of the Mars prime meridian at epoch J2000
- \dot{W} : Rotation rate
- T : Centuries past J2000 (TDB)
- d : Days past J2000 (TDB) .

Since the MRP have a certain accuracy on the one hand, but are treated as constants in our study on the other hand, the Mars-fixed position and attitude parameters are affected by additional errors.

4 GLOBAL BLOCK TRIANGULATION

4.1 Mathematical model

The mathematical model of bundle block triangulation is based on the well-known collinearity equations (e.g. Slama et al., 1980)

$$u_x = u_x^p - c \frac{d_{11}(X - X^c) + d_{21}(Y - Y^c) + d_{31}(Z - Z^c)}{d_{13}(X - X^c) + d_{23}(Y - Y^c) + d_{33}(Z - Z^c)}$$

$$u_y = u_y^p - c \frac{d_{12}(X - X^c) + d_{22}(Y - Y^c) + d_{32}(Z - Z^c)}{d_{13}(X - X^c) + d_{23}(Y - Y^c) + d_{33}(Z - Z^c)} \quad (4)$$

with

- u_x, u_y : Image coordinates of a tie/control point P
- u_x^p, u_y^p : Image coordinates of the principle point P^p
- c : Calibrated focal length
- X^c, Y^c, Z^c : Object coordinates of perspective centers
- d_{11}, \dots, d_{33} : Elements of the orientation matrix represented by three independent angles ϕ, ω, κ
- X, Y, Z : Object coordinates of P

which relate the observed image coordinates u_x, u_y to the unknown object coordinates X, Y, Z of the point P and the unknown parameters of exterior orientation $X^c, Y^c, Z^c, \phi, \omega, \kappa$ of the image. In addition, the interior orientation parameters u_x^p, u_y^p, c can be estimated using the concept of self-calibration (Ebner, 1976).

The positions of all images are treated independently in this model, even if the images were taken from one common orbit. No orbital constraints were used at that time, in future, however, an advanced approach will be integrated which guarantees that all exposure stations of one orbit lie on a physically consistent trajectory. This advanced approach of bundle adjustment will allow us to estimate the MRP as well.

Additional observation equations are formulated for the position, attitude and interior orientation parameters as well as for the object coordinates of MPF which is introduced as GCP.

The occultation data are available as ground points with their latitude φ , longitude λ and radius r coordinates. Since φ and λ have a poor accuracy, only the radii r are incorporated into the bundle adjustment as observations with a certain standard deviation. The occultation points themselves cannot be identified in the VO images, so that each occultation point must be related to the nearest neighbouring tie point, assuming no significant height difference between these two points.

4.2 Input data

For the final block triangulation, various input data were introduced (Table 1). The image coordinates of tie and control points have a priori standard deviations of $\sigma = 10 \mu\text{m}$ or 0.85 pixel. The object coordinates of MPF were assigned with $\sigma = 30 \text{ m}$ each in X, Y, Z as specified by Folkner et al. (1997). The positions of all Viking images were introduced with $\sigma = 5 \text{ km}$, where the accuracy of the inertial trajectory and the influence of the MRP, which are only known with a limited accuracy, are accounted for. The Viking attitude angles were incorporated into the adjustment with their rather poor accuracy of $\sigma = 0.5 \text{ gon}$. In the former block adjustments at RAND and USGS, the attitude angles were introduced with $\sigma = 0.25$, but in our case this value leads to slightly poorer results. The occultation radii are included in the bundle block adjustment with $\sigma = 500 \text{ m}$ according to Smith and Zuber (1996).

Finally, the interior orientation parameters u_x^p, u_y^p, c of the 4 Viking Orbiter cameras (VO-1A, VO-1B, VO-2A, VO-2B) were treated

as free unknowns ($\sigma = \infty$) in the first adjustment run, whereas the interior orientation parameters of the two Mariner 9 images, which are only needed due to Airy-0, were assumed as error-free ($\sigma = 0$). In the subsequent runs, those 5 parameters which were estimated not significantly, have been fixed with $\sigma = 0$, whereas the remaining 7 parameters still have been treated as free unknowns.

observations		type	$\sigma_{a \text{ priori}}$
3739	tie points	image coordinates	10 μm
1	control point	image coordinates	10 μm
1	control point	object coordinates	30 m
1140×3	positions	ext. orient. param.	5 km
1140×3	attitude angles	ext. orient. param.	0.5 gon
246	occultation pts.	radii	500 m
6×3	u_x^p, u_y^p, c	int. orient. param.	$\infty, 0$

Table 1: Input data for global block triangulation

5 RESULTS

5.1 Block triangulation results

After 5–6 iterations final results were achieved. Table 2 shows the standard deviations a priori, the rms values of the residuals and the standard deviations a posteriori of the observations as well as the rms values of the standard deviations of the estimated unknowns for the 6 exterior orientation parameters. It can be seen that the position parameters are improved only slightly by the block adjustment, whereas the attitude parameters are improved considerably due to geometric strength of the closed block.

param.	$\sigma_{a \text{ priori}}$	rms(resid.)	$\sigma_{a \text{ posteriori}}$	rms($\hat{\sigma}$)
X^c [m]	5000	1350	4615	4511
Y^c [m]	5000	1610	4615	4513
Z^c [m]	5000	1124	4615	4531
ϕ [gon]	0.500	0.261	0.461	0.050
ω [gon]	0.500	0.161	0.461	0.038
κ [gon]	0.500	0.238	0.461	0.078

Table 2: Standard deviations a priori, rms values of the residuals and standard deviations a posteriori of the observations as well as rms values of the standard deviations of the estimated unknowns for the exterior orientation parameters

The rms value of the residuals of the observed occultation radii amounts to 197 m. This value is less than half of the a priori standard deviation (500 m) and indicates that the introduced occultation radii fit very well with the photogrammetric block.

Table 3 shows the 7 estimated interior orientation parameters with standard deviations and the significance of their values. The accuracy of the estimated focal lengths is as good as or even exceeds the accuracy figures of the former lab calibration (Benesh and Thorpe, 1976).

camera	param.	value [mm]	$\hat{\sigma}$ [mm]	value / $\hat{\sigma}$
VO-1A	Δc	0.195	0.021	9.25
	x_0	-0.209	0.076	2.76
	y_0	-0.524	0.058	9.03
VO-1B	x_0	-0.257	0.082	3.14
	y_0	-0.389	0.061	6.39
VO-2A	Δc	-0.164	0.042	3.87
VO-2B	Δc	0.354	0.040	8.84

Table 3: Results of self-calibration: estimated interior orientation parameters with their standard deviations and the significance check

These results lead to new sets of calibrated focal lengths and pixel coordinates of the principle points for the 4 VO cameras as given in Tables 4 and 5.

camera	c [mm]	$\hat{\sigma}$ [mm]	remark
VO-1A	474.593	0.021	changed
VO-1B	474.448	0.035	unchanged
VO-2A	474.446	0.042	changed
VO-2B	474.455	0.040	changed

Table 4: New calibrated focal lengths c with their standard deviations for the 4 VO cameras.

camera	column	$\hat{\sigma}$	row	$\hat{\sigma}$	remark
VO-1A	607.24	6.46	619.54	4.93	changed
VO-1B	603.15	6.97	608.07	5.18	changed
VO-2A	625.00	?	575.00	?	unchanged
VO-2B	625.00	?	575.00	?	unchanged

Table 5: New pixel coordinates of the principle points with their standard deviations for the 4 VO cameras.

The rms values $\mu_{\hat{X}}$, $\mu_{\hat{Y}}$ and $\mu_{\hat{Z}}$ of the theoretical standard deviations of the adjusted object point coordinates are nearly equal and amount to 747 m, 772 m and 709 m. The achieved accuracy of the ground points is close to the theoretical accuracy limit of 520 m in X , Y and Z , where error-free orientation parameters are assumed. The maximum theoretical standard deviations are about 3458 m, 4562 m and 2860 m in X , Y and Z .

The global bundle block adjustment was performed using the software package CLIC (TUM 1992) on a Silicon Graphics Power Challenge XL workstation. Depending on the machine load, the complete computation needed 5.5 h on average.

5.2 Discussion of block triangulation results

The results described in the previous section are consistent and show that the simultaneous global 3D block triangulation worked properly with the old and new input data. All available and useful data has been applied. As Table 2 shows, the positions of the VO images were not changed very much, but the attitude parameters of the images were improved considerably due to the geometry of the closed global block. Seven interior orientation parameters of the 4 VO cameras can be improved by self-calibration (see Table 3). This new global block triangulation leads to homogeneous ground point accuracies of about 750 m in all three components X , Y and Z , which is a quite remarkable result. This set of orientation parameters and ground points may now be used for DTM generation and mapping purposes as well as for current (Mars Global Surveyor 1996) and future (e.g. Mars Surveyor 1998 and 2001, Mars Express 2003) missions to Mars.

The standard deviations of the adjusted object coordinates of the control point MPF are nearly equal to the corresponding a priori values. Thus the object coordinates of MPF can not be improved by the block triangulation. The final ground coordinates of MPF and, in addition, VL1 and Airy-0 are given in Table 6.

The longitude coordinate $\hat{\lambda}$ of Airy-0 is now not equal to zero, but -0.2015 . Note that this crater previously has been defined the 0° meridian of Mars. But with the change of the rotational parameters, this definition is no longer valid, and it is not surprising that the $\hat{\lambda}$ coordinate is not exactly equal to zero.

Table 7 shows the differences between the well-determined object coordinates from Folkner et al. (1997) and the adjusted object coordinates from the block triangulation for VL1. Due to the identification error, these differences amount to about 5 km.

5.3 Comparison with former USGS network

A first comparison of the resulting object coordinates of the tie points with the former coordinates determined by USGS was made by computing the differences between the old and new coordinates for each identical point. The rms values of the differences amount

point	\hat{X} [km]	\hat{Y} [km]	\hat{Z} [km]
MPF	2670.37	-1769.07	1108.90
VL1	2087.41	-2343.67	1283.10
Airy-0	3380.62	-11.89	-300.38
	$\hat{\phi}$ [°]	$\hat{\lambda}$ [°]	\hat{h} [m]
MPF	19.3267	-33.5237	-4909.5
VL1	22.4985	-48.3100	-3183.0
Airy-0	-5.1437	-0.2015	-2860.2

Table 6: Adjusted Cartesian and ellipsoidal object coordinates of MPF, VL1 and Airy-0. \hat{h} denotes the height above the IAU ellipsoid from 1973.

point	ΔX [km]	ΔY [km]	ΔZ [km]
VL1	2.30	4.68	1.31
	$\Delta\phi$ [°]	$\Delta\lambda$ [°]	Δh [m]
VL1	0.0333	0.0875	-1299.4

Table 7: Differences between the known and the adjusted Cartesian and ellipsoidal object coordinates of VL1. \hat{h} denotes the height above the IAU ellipsoid from 1973.

to 9767 m in X , 8842 m in Y and 2287 m in Z . These differences may be mainly explained by a rotation around the Z -axis of the Mars-fixed object coordinate system. Since the old USGS coordinates refer to the network determined by M. Davies in 1978 (Davies et al., 1978), the obsolete value for W_0 is still relevant. The difference between the 1978 and the 1997 value of W_0 now causes this rotation around the Z -axis.

A second, more detailed comparison was based on a spatial (7 parameter) similarity transformation between both datasets. To this end, the old USGS coordinates were transformed into the new coordinates derived from this study. The resulting parameters of the adjustment with 3180 identical points are summarized in Table 8.

parameter	value	σ
$\Delta \hat{X}$ [m]	-771	31
$\Delta \hat{Y}$ [m]	382	31
$\Delta \hat{Z}$ [m]	582	31
$\hat{\epsilon}_x$ [°]	-0.0176	0.00064
$\hat{\epsilon}_y$ [°]	-0.0227	0.00066
$\hat{\epsilon}_z$ [°]	-0.2623	0.00064
\hat{m}	1.0000537	0.0000092

Table 8: Results of a 7 parameter transformation between the coordinates of the old USGS and the new Mars net

The shift parameters $\Delta \hat{X}$, $\Delta \hat{Y}$, $\Delta \hat{Z}$, the rotations $\hat{\epsilon}_x$, $\hat{\epsilon}_y$ and the scale factor \hat{m} do not show any systematic effects, whereas $\hat{\epsilon}_z$ indicates a significant rotation around the Z -axis. This rotation $\hat{\epsilon}_z$ can be explained by the change of the rotational parameter W_0 as already mentioned. The remaining residuals between both coordinate sets after the transformation amount to 1470 m, 1950 m and 1810 m in X , Y and Z (rms values). These values compared with $\sigma = 750$ m of our new coordinates indicate that the accuracy of the Mars network is improved at least by factor 2.

5.4 New reference bodies

Based on the new Mars network reference bodies related to the center of mass can be determined. The simplest reference body is a sphere characterized by its radius r . For each object point of the Mars net the radius from the origin of the coordinate system (center of mass) to the surface point can be easily computed. Fitting all these values together, a mean radius

$$r = 3390.78 \pm 0.10 \text{ km}$$

of a reference sphere was found.

A more advanced reference body to describe the shape of Mars is an oblate ellipsoid or spheroid

	sphere	spheroid	3-axial ellipsoid
X_0 [km]	-0.08 ± 0.17	-1.52 ± 0.08	-1.14 ± 0.07
Y_0 [km]	-2.13 ± 0.18	-1.05 ± 0.08	-0.88 ± 0.07
Z_0 [km]	-2.52 ± 0.19	-3.38 ± 0.08	-3.31 ± 0.08
r [km]	3390.48 ± 0.10	—	—
a [km]	—	3396.53 ± 0.07	3394.20 ± 0.10
b [km]	—	3376.85 ± 0.12	3398.82 ± 0.10
c [km]	—	—	3376.90 ± 0.12

Table 9: Parameters of the reference figures, where the center coordinates were treated as additional unknowns.

$$\frac{X_i^2}{a^2} + \frac{Y_i^2}{a^2} + \frac{Z_i^2}{b^2} = 1 \quad (5)$$

with the two axes a and b . In a least squares adjustment, the axes a and b were estimated from the object coordinates $X_i, Y_i, Z_i (i = 1, \dots, 3740)$ to

$$a = 3396.10 \pm 0.08 \text{ km} \quad \text{and} \quad b = 3377.40 \pm 0.15 \text{ km} .$$

These values can be interpreted as a refinement of the current IAU-values ($a = 3393.4 \text{ km}$, $b = 3375.8 \text{ km}$) of de Vaucouleurs et al. (1973).

Another reference body is a 3-axial ellipsoid

$$\frac{X_i^2}{a^2} + \frac{Y_i^2}{b^2} + \frac{Z_i^2}{c^2} = 1 \quad (6)$$

with the 3 axes a, b and c . For this case, the 3 axes were estimated to

$$a = 3393.45 \pm 0.12 \text{ km}, \quad b = 3398.88 \pm 0.12 \text{ km} \quad \text{and} \quad c = 3377.42 \pm 0.14 \text{ km} .$$

5.5 Offset between center of figure and center of mass

Another characteristic of Mars is the remarkable offset between the center of figure (COF) and the center of mass (COM), which is in the order of about 3 km towards the South (Smith and Zuber, 1996). Depending on the chosen reference body, different values for this offset may be achieved.

In our case we used the object coordinates X_i, Y_i, Z_i of the Mars net and fitted a sphere, a spheroid and a 3-axial ellipsoid where the center coordinates X_0, Y_0, Z_0 were treated as additional unknowns. The formula for a 3-axial ellipsoid reads:

$$\frac{(X_i - X_0)^2}{a^2} + \frac{(Y_i - Y_0)^2}{b^2} + \frac{(Z_i - Z_0)^2}{c^2} = 1 \quad (7)$$

The results of the three adjustments are listed in Table 9. These values demonstrate that the offset between COF and COM is significant, mainly in the Z -direction. The results are similar to those of Smith and Zuber (1996). Differences between the results of the two studies may be explained by different input data which were used for the computations.

6 SUMMARY AND OUTLOOK

In our study the existing control point network of Mars was recomputed using 80% of the original image coordinates of USGS tie points, new image coordinates of ground control points (VL1 and MPF) and other available data. Corrected image time tags were incorporated as well as improved Viking orbit trajectories, present Mars rotational parameters, the Pathfinder landing site and re-analysed occultation data. All this heterogeneous information was combined within a consistent simultaneous 3D bundle block adjustment. This effort yielded an improved set of image positions and

attitudes, interior orientation parameters of the 4 VO cameras and object coordinates of the tie points with $\sigma \sim 750 \text{ m}$ in X, Y, Z .

Using these results, heights referring to the gravity field model Mars50c can be computed, local, regional and global DTMs can be derived and parameters of reference bodies can be determined.

In near future, the bundle adjustment model will be extended by orbital constraints to exploit the fact that all camera positions lie on a physical orbit trajectory (Montenbruck et al., 1994; Ohlhof, 1996). The Mars rotational parameters will be estimated in the extended bundle adjustment too. Global Surveyor data may improve the results of this adjustment due to the new image data from MOC and the very precisely measured height profiles from MOLA. It is also possible to combine the Global Surveyor and Viking data within a common global block adjustment. The mathematical model to incorporate MOLA data into the bundle adjustment can be found in Ebner and Ohlhof (1994).

7 ACKNOWLEDGEMENTS

We wish to thank R. Kirk (USGS), M. Davies (RAND) and T. Duxbury (JPL) for providing us image coordinates used in this study. C. Acton and B. Semenov (JPL) provided important Viking orbit, attitude and image time tag information, W. Folkner (JPL) the new Mars rotational parameters, and D. Smith (GSFC) the re-analysed radio occultation data. J. Oberst (DLR-PE), E. Gill (DLR-GSOC) and J.-P. Muller (UCL) contributed helpful discussions to our work.

8 REFERENCES

- Benesh M., Thorpe T. (1976): *Viking Orbiter 1975 Visual Imaging Subsystem Calibration Report*; JPL Publication 611-125, 253.
- De Vaucouleurs G.M., Davies M.E., Sturms M. Jr. (1973): *Mariner 9 Areographic Coordinate System*; JGR **78**, 4395-4404.
- Davies M.E., Berg R.A. (1971): *A Preliminary Control Net of Mars*; JGR **76**, 373-393.
- Davies M.E., Katayama F.Y., Roth J.A. (1978): *Control Net of Mars: February 1978*; Report R-2309-NASA, The Rand Corporation, Santa Monica.
- Davies M.E. (1993): *The Coordinate System and Control Network of Mars*; Presentation at the 3rd HRSC/WAOSS Photogrammetry and Cartography Working Group Meeting, May 12-14, 1993, Berlin.
- Ebner H. (1976): *Self Calibrating Block Adjustment*; BuL **44**(4), 128-139.
- Ebner H., Ohlhof T. (1994): *Utilization of Ground Control Points for Image Orientation Without Point Identification in Image Space*; IntArchPhRS **30**(3), 206-211.
- Folkner W.M., Yoder C.F., Yuan D.N., Standish E.M., Preston R.A. (1997): *Interior structure and seasonal mass redistribution of Mars from radio tracking of Mars Pathfinder*; Science **278**, 1749-1752.
- Konopliv A.S., Sjogren W.L. (1995): *The JPL Mars Gravity Field, Mars50c, Based Upon Viking and Mariner 9 Doppler Tracking data*; JPL Publication 95-5.

- Michael W.H. Jr. (1979): *Viking Lander Tracking Contributions to Mars Mapping*; The Moon and the Planets **20**, 149-152.
- Ohlhof T. (1996): *Lokale, regionale und globale Punktbestimmung mit Dreizeilenbilddaten und Bahninformation der Mars96-Mission*; PhD thesis, Deutsche Geodätische Kommission, C 445, 139 p.
- Montenbruck O., Gill E., Ohlhof T. (1994): *A Combined Approach for Mars-94 Orbit Determination and Photogrammetric Bundle Adjustment*; DLR Research Report 94-13, 95 p.
- Morris E.C., Jones K.L. (1980): *Viking 1 Lander on the Surface of Mars: Revised Location*; Icarus **44**, 217-222.
- Slama C. et al. (1980): *Manual of Photogrammetry*; 4th edition, American Society of Photogrammetry, 1056 p.
- Smith D.E., Zuber M.T. (1996): *The Shape of Mars and the Topographic Signature of the Hemispheric Dichotomy*; Science **271**, 184-188.
- TUM (1992): *CLIC — Bundle Block Adjustment Program. Product Information and User's Manual*; Chair for Photogrammetry and Remote Sensing, Technische Universität München.
- Wu S.S.C., Doyle F.J. (1990): *Topographic Mapping*; in: Planetary Mapping, edited by R. Greeley and R. Batson, Cambridge Planetary Science Series 6, 169-207.